ARTICLE NO. 79-1706R

G80-059

Azimuth Observability Enhancement During Inertial Navigation System In-Flight Alignment

00016
00021
00022

Itzhack Y. Bar-Itzhack* and Boaz Porat†
Technion—Israel Institute of Technology, Haifa, Israel

This paper addresses the question whether a constant axial acceleration maneuver is superior to a circular one during the in-flight alignment of an inertial navigation system and whether there exists a simple test or an expression that clearly indicates it. It was found in this work that when the azimuth misalignment at the end of the maneuver is the index of performance, the axial maneuver is not superior to the lateral one in general. There are, however, three classes of alignment problems in which axial maneuver is superior. These cases can be modeled by simple models that yield analytic expressions clearly indicating the superiority of the axial maneuver during the in-flight alignment of an inertial navigation system. These three classes of alignment problems encompass a large number of existing systems.

Introduction

ANY inertial navigation system (INS) has to undergo an initial alignment phase before it starts navigating. During this phase the attitude difference between the axes of the INS coordinate system and those of a chosen reference is estimated and removed. This attitude difference, or misalignment, consists of two tilt angles and an azimuth angle which have a distinct signature in the propagating error in the INS outputs. For this reason a Kalman filter can be successfully used to estimate the tilt and the azimuth errors of the INS. It is well known that the estimation rate of the azimuth misalignment and the final value it reaches are the two factors that determine the performance of the whole alignment process. These factors are particularly important in the initial alignment of the INS of a combat aircraft, where the aircraft has to be ready for takeoff in minimum time.

The initial alignment can be performed either when the INS is at rest or while the aircraft is in motion.[1] If the initial alignment is carried out when the INS is airborne, the alignment is referred to as in-flight alignment (IFA). Classically, the INS outputs that are used to estimate the tilt and the azimuth errors are the two horizontal velocity error components. The tilt errors are strongly correlated with these velocity error components, and thus can be easily estimated. An issue of major importance, then, is the "observability magnitude" of the azimuth misalignment angle when the horizontal velocity error components are measured.

To present the observability problem, we turn to Eq. (1), which is the propagation equation of the horizontal velocity error and the misalignment components for an INS whose reference coordinate system is the local level north pointing system[2]:

$$\frac{d}{dt}\begin{bmatrix} v_N \\ v_E \\ \phi_N \\ \phi_E \\ \phi_D \end{bmatrix} = \begin{bmatrix} 0 & -(2\Omega+\dot{\lambda})\sin L & 0 & -a_D(t) & a_E(t) \\ (2\Omega+\dot{\lambda})\sin L & 0 & a_D(t) & 0 & -a_N(t) \\ 0 & 1/R & 0 & -(\Omega+\dot{\lambda})\sin L & \dot{L} \\ -1/R & 0 & (\Omega+\dot{\lambda})\sin L & 0 & (\Omega+\dot{\lambda})\cos L \\ 0 & -\tan L/R & -\dot{L} & -(\Omega+\dot{\lambda})\cos L & 0 \end{bmatrix} \begin{bmatrix} v_N \\ v_E \\ \phi_N \\ \phi_E \\ \phi_D \end{bmatrix} + \begin{bmatrix} \nabla_N \\ \nabla_E \\ \epsilon_N \\ \epsilon_E \\ \epsilon_D \end{bmatrix} \quad (1)$$

v_N and v_E are, respectively, the north and east components o the velocity error. $a_N(t)$, $a_E(t)$, and $a_D(t)$ are the north, east, and down components of the sensed acceleration. ϕ_N, ϕ_E, and ϕ_D are the north, east, and down components of the misalignment. Ω denotes Earth rate, R is the radius of the Earth, and L and λ are, respectively, the latitude and longitude of the INS. ∇_N and ∇_E are the north and east accelerometer error terms, whereas ϵ_N, ϵ_E, and ϵ_D are, respectively, the drifts of the north, east, and down gyros. The vertical channel of the INS is decoupled from the horizontal channels, thus its error terms do not appear in Eq. (1). It is assumed that the INS is at a constant altitude, therefore the nominal values of the vertical channel do not appear in Eq. (1) either.

Consider the 5×5 matrix in Eq. (1) which is the error dynamics matrix that we denote by F_5. When ground alignment is performed, that is, when the INS is stationary, the sensed acceleration is in the vertical direction and is equal to the gravity. Thus, only the tilt errors ϕ_N and ϕ_E are directly coupled into v_E and v_N through the gravity of $f_{2,3}$ and $f_{1,4}$, respectively ($f_{i,j}$ denotes the element in the ith row and the jth column of F_5). This coupling is a strong one since the gravity is a relatively large quantity. On the other hand, the azimuth error ϕ_D is not coupled directly into either v_N or v_E; however, it is coupled indirectly into v_N as follows: ϕ_D is coupled directly into ϕ_E through $f_{4,5}$ which is the north component of Earth rate and, as was just mentioned, ϕ_E is coupled into v_N through the gravity of $f_{1,4}$; consequently, v_N is linked to ϕ_D. Because of the difference in the nature of the coupling of ϕ_D and ϕ_E into v_N, they have different signatures in v_N and are separable and observable to the Kalman filter. However, since ϕ_D first has to excite ϕ_E in order to excite v_N, and since the coupling between ϕ_D and ϕ_E is a weak one, as Earth rate has a small magnitude, the estimation of the azimuth error takes longer, which is well known.

Now, if the INS is installed on a maneuverable aircraft and the initial alignment is carried out while the aircraft is air-

Received April 24, 1979; presented as Paper 79-1706 at the AIAA Guidance and Control Conference, Boulder, Colo., Aug. 6-8, 1979; revision received Nov. 7, 1979.

Index categories: Guidance and Control; Military Missions; Navigation, Communication, and Traffic Control.

*Associate Professor, Dept. of Aeronautical Engineering. Member AIAA.

†Graduate Student, Dept. of Aeronautical Engineering.

borne, the azimuth misalignment can be made to influence v_N and v_E directly. This is accomplished by maneuvering the aircraft to generate horizontal accelerations in either the northern direction or the eastern direction, or both. This way the elements $f_{2,5}$ or $f_{1,5}$, or both, couple ϕ_D directly into either v_E or v_N, or both, respectively. A commonly recommended flight profile for IFA is a relatively short period of cruising, during which the tilt angles are rapidly estimated, followed by either *S*-turns or a circular flight which generate lateral accelerations to estimate the azimuth misalignment angle ϕ_D. An alternate procedure is to replace the curved portion of the flight path by a straight path on which the aircraft undergoes axial accelerations.

Misalignment observability enhancement through aircraft maneuvers was presented in the past in several places.[3-7] Results presented in a recent paper[8] indicate that axial acceleration maneuvers are superior to lateral acceleration maneuvers. While Ref. 8 analyzes a special case, namely, a strap-down INS mounted on a tactical vehicle, the implication of the results is quite general.

Problem Statement

Although it was indicated in the literature that an axial acceleration maneuver is superior to a lateral one in enhancing the estimation of the INS azimuth misalignment, to our knowledge, this fact was never substantiated analytically. *The primary purpose of this work, therefore, is to find an analytical proof that this contention is correct.* Since it seems that there is a basic truth underlying this phenomenon, regardless of the practicality of the maneuvers that generate the accelerations, in this analysis we prefer to use accelerations that are easy to handle analytically. For this reason the family of axial accelerations is represented in the ensuing analysis by a constant axial acceleration and the family of lateral accelerations is represented by the centrifugal acceleration generated on a circular maneuver. For a fair comparison, though, we have made the magnitudes of these accelerations equal. Naturally, this work does not concern itself with the question of finding an optimal maneuver to fit a certain mission, nor does it deal with the practical aspects of the maneuvers.

Following the primary goal of this work, a simple test was sought that could yield a conclusive analytical indication that axial accelerations are superior to lateral ones. In this context the equation

$$\dot{\vec{v}}=\vec{a}\times\vec{\phi} \tag{2}$$

was investigated. This equation, in which $\vec{a}$ is the vector of sensed acceleration, is a good approximation of the model[9] that describes the INS velocity error propagation due to misalignment. Since $\vec{\phi}$ is a vector of constant angles, an integration of Eq. (2) reveals that the horizontal component of $\vec{v}$ is equal to the product of the aximuth misalignment angle and the norminal velocity change of the INS. As mentioned above, the horizontal component of $\vec{v}$ is the quantity used to estimate ϕ_D; therefore, the larger the change in the nominal velocity, the faster the estimation process of ϕ_D. There is obviously a much greater net velocity change with a constant axial rather than a lateral acceleration maneuver; therefore, axial acceleration maneuver is superior to a lateral one. This heuristic explanation is incomplete: it does not yield a rigorous proof, nor does it produce quantitative results through which the influence of both accelerations can be compared.

We have adopted a different approach for investigating the difference between the influence axial and lateral acceleration maneuvers have on azimuth error estimation during IFA. In order to confirm our results, we used a covariance simulation of the IFA problem. This simulation and its results are presented first.

Full Model Covariance Simulation

The dynamic model used in the simulation is that of a simple standard INS error model which is the result of the augmentation of Eq. (1) with the dynamic model of the sensor error propagation. We assume that the dominant error component in the sensors is the turn-on to turn-on random constant; that is, a constant bias in the accelerometers and a constant drift in the gyros. Recalling that F_5 denotes the dynamics matrix of Eq. (1), the augmented INS error propagation model is given by

$$\dot{x}=Fx+w \tag{3}$$

where

$$F=\left[\begin{array}{c|c} F_5 & I_5 \\ \hline 0 & 0 \end{array}\right] \tag{4}$$

and I_5 is a fifth-order identity matrix. The components of x are as follows:

$$x^T=[v_N,v_E,\phi_N,\phi_E,\phi_D,\nabla_N,\nabla_E,\epsilon_N,\epsilon_E,\epsilon_D] \tag{5}$$

and those of w are

$$w^T=[0,0,0,0,0,w_{\nabla N},w_{\nabla E},w_{\epsilon N},w_{\epsilon E},w_{\epsilon D}] \tag{6}$$

where T denotes the transpose. The nonzero components of w are small-amplitude white noise driving signals which add a small random-walk component to the sensor random constant to simulate the additional, relatively small, sensor errors.

The measured quantities are v_N and v_E and the measurement accuracy is assumed to be 0.2 m/s. We assume that a measurement is made every 4 s, which constitutes a sampling interval much shorter than the period of the INS (84.5 min). Thus, to simplify the simulation, a continuous Kalman filter is simulated; that is, the following matrix Riccati equation is solved:

$$\dot{P}=FP+PF^T+Q-PH^TR^{-1}HP \tag{7}$$

where P is the estimation error covariance matrix, Q is the spectral density matrix that corresponds to the white noise vector w, and R is the spectral density matrix of the white noise measurement error.

Two classes of runs were made. The division into the classes is according to the two kinds of representative maneuvers that were used in the simulation. The first kind, the lateral acceleration maneuver, started with a cruising segment followed by a circular flight path during which the aircraft pulled a lateral constant magnitude accleration. The maneuver terminated with a final cruising segment. The second kind, the axial acceleration maneuver, started also with a crusing segment which was followed by an axial constant-acceleration flight path. This maneuver, too, terminated with a final cruising segment. Numerous runs were made with a wide spectrum of initial conditions in which both kinds of maneuvers were employed.

In most of the runs, at the end of the final cruising segment, axial acceleration was better; that is, the azimuth misalignment estimation error reached a lower level. This, however, was not true when we observed the azimuth error at the end of the accelerating portion of the flight trajectory. There we observed two general groups of outcomes.

1) If both the initial misalignment errors and the initial gyro constant drifts were large and no certain special relations existed among them, we observed that *lateral* acceleration was superior to axial acceleration. These cases belong to group number one.

2) In the following cases, which belong to group number two, *axial* acceleration was superior.

a) The initial gyro drift rates were small.
b) The initial gyro *constant* drift rates were large but

$$\dot{L}\phi_D \ll \epsilon_D \quad \text{and} \quad \tilde{\Omega}_D\phi_D \ll \epsilon_D \tag{8}$$

where

$$\tilde{\Omega}_D = (\Omega + \dot{\lambda})\cos L$$

c) The gyro *constant* drift rates were large but the azimuth gyro drift rate was several times larger than the other two.

Note that cases a and b of group number two encompass many practical problems. The initial alignment of high-quality platforms ($\simeq 1$ n.mi/h) falls into the first case. Typical to the second case is an INS whose gyro drifts are too large for the desired azimuth alignment accuracy and, therefore, the alignment is performed optically. In this case the IFA serves mainly as a means for gyro calibration.

The behavior of the estimated azimuth misalignment in runs belonging to group number one was found to be quite erratic. The results at the beginning and at the end of the final cruising segment contradicted one another; namely, at the beginning of the segment the lateral acceleration maneuver seemed to have been superior, while at the end of the cruising segment the axial acceleration maneuver yielded a smaller azimuth misalignment estimation error. No simple analytical model was found for this group (i.e., for the corresponding class of initial conditions).

In the following sections, it will be shown that a simple model can be found for the second group of outcomes that yields analytic expressions that clearly indicate the superiority of axial acceleration at the end of the accelerating segment of the IFA trajectory. In fact, there are two such models; one is a third-order model for merely estimating ϕ_D (case a), and the second model is a fourth-order one for estimating ϕ_D as well as ϵ_D (cases b and c).

Third-Order Model

We postulate that in the first case of group number two, the error propagation of the horizontal velocity components is distinctly governed by the azimuth misalignment angle ϕ_D whose value we wish to estimate, and since ϵ_D is fairly small, ϕ_D is constant. Consequently, the full-order INS error propagation model can be replaced by the following third-order model:

$$\dot{x}_3 = F_3(t)x_3 \tag{9}$$

where

$$x_3^T = [v_N, v_E, \phi_D] \tag{10}$$

and

$$F_3(t) = \begin{bmatrix} 0 & 0 & a_E(t) \\ 0 & 0 & -a_N(t) \\ 0 & 0 & 0 \end{bmatrix} \tag{11}$$

The measurement matrix H_3 is obviously

$$H_3 = \begin{bmatrix} 1 & 0 & 0 \\ 0 & 1 & 0 \end{bmatrix} \tag{12}$$

and

$$R = \begin{bmatrix} \sigma_v^2 & 0 \\ 0 & \sigma_v^2 \end{bmatrix} \tag{13}$$

Assuming no a priori information on x_3, the covariance matrix of the system at any time $P_3(t)$ can be found as follows[10,11]:

$$P_3(t) = \left\{ \int_0^t \Psi_3^T(\tau,t) H_3^T R^{-1} H_3 \Psi_3(\tau,t)\, d\tau \right\}^{-1} \tag{14}$$

where $\Psi_3(\tau,t)$ is the transition matrix that corresponds to $F_3(t)$.

Note that the integral is the *stochastic observability matrix* of the system. The system is said to be uniformly completely observable when the integral is positive definite and bounded for some $t > 0$. We are further interested in a quantitative measure of the observability of ϕ_D which may be used to compare the effect of the lateral maneuver with that of the axial maneuver. A good quantitative measure for this reason is the variance of the estimation error of ϕ_D which is $p_3(3,3,)$, the 3,3, element of $P_3(t)$. Using Eq. (14) we now proceed to compute $p_3,(3,3)$ for the lateral as well as for the axial maneuver.

Lateral Maneuvers

A circular path generates the following components of sensed acceleration

$$a_N(t) = -A \cdot \sin\omega t \qquad a_E(t) = A \cdot \cos\omega t \tag{15}$$

where A is the magnitude of the lateral acceleration. Substituting Eqs. (15) into Eq. (11) yields

$$F_3(t) = \begin{bmatrix} 0 & 0 & A\cos\omega t \\ 0 & 0 & A\sin\omega t \\ 0 & 0 & 0 \end{bmatrix} \tag{16}$$

$\Psi_3(t,t_0)$ is the solution of

$$\frac{\partial}{\partial t}\Psi_3(t,t_0) = F_3(t)\Psi_3(t,t_0) \qquad \Psi_3(t_0,t_0) = I \tag{17}$$

which is

$$\Psi_3(t,t_0) = \begin{bmatrix} 1 & 0 & (A/\omega)(s\omega t - s\omega t_0) \\ 0 & 1 & (A/\omega)(c\omega t_0 - c\omega t) \\ 0 & 0 & 1 \end{bmatrix} \tag{18}$$

where s denotes the sine function and c the cosine function. Using Eqs. (12), (13), and (18), $g_3(\tau,t)$—the integrand of Eq.

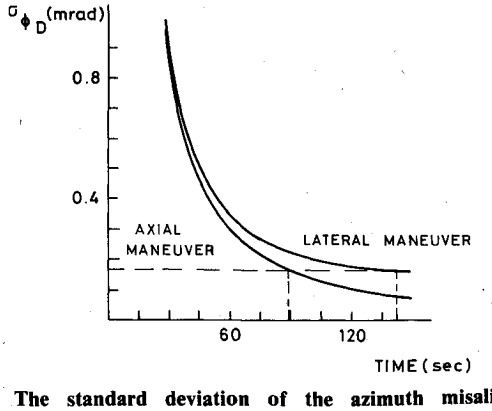

Fig. 1 The standard deviation of the azimuth misalignment estimation error derived from the third-order analytic model.

(14)—is obtained as follows:

$$g_3(\tau,t)=\frac{1}{\sigma_v^2}\begin{bmatrix}1 & 0 & (A/\omega)(s\omega\tau-s\omega t)\\ 0 & 1 & (A/\omega)(c\omega t-c\omega\tau)\\ (A/\omega)(s\omega\tau-s\omega t) & (A/\omega)(c\omega t-c\omega\tau) & (2A^2/\omega^2)[1-c\omega(t-\tau)]\end{bmatrix} \tag{19}$$

Following Eq. (14), the integration of $g_3(\tau,t)$ with respect to τ between the limits 0 and t yields

$$P_3^{-1}(t)=\frac{1}{\sigma_v^2}\begin{bmatrix}t & 0 & (A/\omega^2)(1-\omega t\cdot s\omega t-c\omega t)\\ 0 & t & (A/\omega^2)(\omega t\cdot c\omega t-s\omega t)\\ (A/\omega^2)(1-\omega t\cdot s\omega t-c\omega t) & (A/\omega^2)(\omega t\cdot c\omega t-s\omega t) & (2A/\omega^3)(\omega t-s\omega t)\end{bmatrix} \tag{20}$$

The determinant of $P_3^{-1}(t)$ is easily found to be

$$\det\{P_3^{-1}(t)\}=(2/\sigma_v^6\omega^5)[(\omega t)^3-(\omega t)\cdot 2(1-c\omega t)] \tag{21}$$

Now from Eq. (20), $P_3(3,3)$—the 3,3 element of $P_3(t)$—is given by

$$P_3(3,3)=t^2/\det\{P^{-1}(t)\}\cdot\sigma_v^4 \tag{22}$$

then substituting Eq. (21) into Eq. (22) yields

$$\sigma_{\phi_D}^2=P_3(3,3)=\frac{\omega^3\sigma_v^2}{A^2}\,\frac{\omega t}{(\omega t)^2-2(1-c\omega t)} \tag{23}$$

Axial Maneuver

With no loss of generality we may assume that the axial acceleration is due north; thus

$$a_N=A \qquad a_E=0 \tag{24}$$

Then Eq. (11) becomes

$$F_3(t)=\begin{bmatrix}0 & 0 & 0\\ 0 & 0 & -A\\ 0 & 0 & 0\end{bmatrix} \tag{25}$$

and the solution of Eq. (17) with this $F_3(t)$ is

$$\Psi_3(t,t_0)=\begin{bmatrix}1 & 0 & 0\\ 0 & 1 & A(t_0-t)\\ 0 & 0 & 1\end{bmatrix} \tag{26}$$

Consequently, the integrand of Eq. (14) is

$$g_3(\tau,t)=\frac{1}{\sigma_v^2}\begin{bmatrix}1 & 0 & 0\\ 0 & 1 & A(t-\tau)\\ 0 & A(t-\tau) & A^2(t-\tau)^2\end{bmatrix} \tag{27}$$

Then, following Eq. (14),

$$P_3^{-1}(t)=\frac{1}{\sigma_v^2}\begin{bmatrix}t & 0 & 0\\ 0 & t & \tfrac{1}{2}At^2\\ 0 & \tfrac{1}{2}At^2 & \tfrac{1}{3}A^2t^3\end{bmatrix} \tag{28}$$

and

$$\det\{P_3^{-1}(t)\}=A^2t^5/12\sigma_v^6 \tag{29}$$

Now from Eq. (28)

$$P_3(3,3)=t^2/\det\{P^{-1}(t)\}\cdot\sigma_v^4 \tag{30}$$

Hence, from Eqs. (29) and (30) we obtain

$$\sigma_{\phi_D}^2=P_3(3,3)=12\sigma_v^2/A^2t^3 \tag{31}$$

For a quick comparison between this result and that of the lateral acceleration, we introduce ω into Eq. (31) as follows:

$$\sigma_{\phi_D}^2=12(\omega^3\sigma_v^2/A^2)\cdot 1/(\omega t)^3 \tag{32}$$

We realize that for large ωt (i.e., for large t) Eq. (32) approaches zero as $1/t^3$ while Eq. (23) approaches zero as $1/t$, and clearly *the axial acceleration maneuver is indeed superior to the lateral acceleration maneuver.* To see the correspondance between these analytic results and simulation results, consider Figs. 1 and 2. Figure 1 presents the difference between σ_{ϕ_D} of Eq. (23) and that of Eq. (32); that is, Fig. 1 presents the difference between the axial and lateral maneuvers obtained from the analytic model. Figure 2, on the other hand, presents the difference between σ_{ϕ_D} of the lateral maneuver and that of the axial maneuver which were obtained from the simulation.

The values which were used in the simulation are

$\omega=0.05$ rad/s $\quad A=9.81$ m/s^2 $\quad \sigma_v=0.4$ m/s/$\sqrt{\text{Hz}}$

$$Q_{(6,6)}=Q_{(7,7)}=1.92\times10^{-13}\text{m}^2/\text{s}^5$$

$$Q_{(8,8)}=Q_{(9,9)}=Q_{(10,10)}=1.88\times10^{-17}\text{rad}^2/\text{s}^3$$

In addition we used the following initial values:

$\sigma_{\epsilon_N}=\sigma_{\epsilon_E}=0.01$ deg/h $\quad \sigma_{\epsilon_D}=0.025$ deg/h

$\sigma_{\phi_N}=\sigma_{\phi_E}=1$ deg $\quad \sigma_{\phi_D}=3$ deg

$\sigma_{\nabla_N}=\sigma_{\nabla_E}=100\ \mu g$ $\quad \sigma_{v_N}=\sigma_{v_E}=0.2$ m/s

Note that the initial conditions of this simulation were chosen to make these examples elements which belong to case a in group number two, for which the suitable analytic model is a third-order one.

Note in Fig. 2 that at the end of the alignment, both curves approach the same value due to the existence of white noise excitation in the simulation. The basic conclusion from the two figures is that shortly after the beginning of the accelerating segment of the flight path, the simple third-order model represents fairly well the alignment process. Therefore, the analytic expressions in Eqs. (23) and (32) are good approximations to the azimuth alignment process which is the governing phenomenon during this stage of the alignment. A

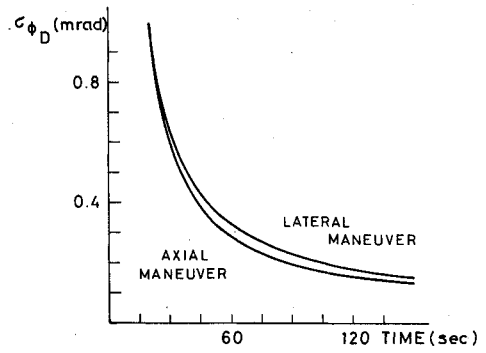

Fig. 2 The standard deviation of the azimuth misalignment estimation error derived from the simulation of case a.

comparison between Eqs. (23) and (32) clearly demonstrates the superiority of the axial maneuver in the enhancement of the azimuth observability, provided that the gyro drifts are small. In our case, for example, it is shown in Fig. 1 that it takes 37% less time to achieve 0.17 mrad when the axial maneuver is employed.

Fourth-Order Model

We now turn our attention to cases b and c of group number two in which the azimuth gyro constant drift rate is not negligible. Here we postulate that the error propagation of the horizontal velocity components is still distinctly governed by ϕ_D. However, due to the existence of the large azimuth gyro constant drift rate, ϕ_D is not constant now. The full-order INS error propagation model is now reduced to the following fourth-order model:

$$\dot{x}=F_4(t)x_4 \tag{33}$$

where

$$x_4^T=[\upsilon_N,\upsilon_E,\phi_D,\epsilon_D] \tag{34}$$

and

$$F_4(t)=\begin{bmatrix}0&0&a_E(t)&0\\0&0&-a_N(t)&0\\0&0&0&1\\0&0&0&0\end{bmatrix} \tag{35}$$

The suitable measurement matrix is

$$H_4=\begin{bmatrix}1&0&0&0\\0&1&0&0\end{bmatrix} \tag{36}$$

and R is that given by Eq. (13). Again, we wish to examine the stochastic observability matrix of this fourth-order system; that is,

$$P_4(t)=\left\{\int_0^t \Psi_4^T(\tau,t)H_4^TR^{-1}H_4\Psi_4(\tau,t)\,d\tau\right\}^{-1} \tag{37}$$

We are interested in $P_4(3,3)$ and $P_4(4,4)$, which are, respectively, the 3,3 and 4,4 elements of $P_4(t)$ since

$$P_4(3,3)=\sigma_{\phi_D}^2 \tag{38}$$

and

$$P_4(4,4)=\sigma_{\epsilon_D}^2 \tag{39}$$

Lateral Maneuver

Substitution of Eqs. (15), the expressions for the sensed acceleration on a circular path, into Eq. (35) yields

$$F_4(t)=\begin{bmatrix}0&0&A\cos\omega t&0\\0&0&A\sin\omega t&0\\0&0&0&1\\0&0&0&0\end{bmatrix} \tag{40}$$

The solution of Eq. (17) for the fourth-order dynamics matrix, Eq. (40) yields

$$\Psi_4(t,t_0)=\begin{bmatrix}1&0&(A/\omega)(\sin\omega t-\sin\omega t_0)&(A/\omega^2)[(\omega t-\omega t_0)\sin\omega t+(\cos\omega t-\cos\omega t_0)]\\0&1&-(A/\omega)(\cos\omega t-\cos\omega t_0)&-(A/\omega^2)[(\omega t-\omega t_0)\cos\omega t-(\sin\omega t-\sin\omega t_0)]\\0&0&1&t-t_0\\0&0&0&1\end{bmatrix} \tag{41}$$

For convenience we make the following change of variables:

$$x=\omega t \qquad y=\omega\tau \tag{42}$$

Then the integrand of Eq. (37), $g_4(\tau,t)$, becomes $g_4^*(y,x)$, and is given by

$$g_4^*(y,x)=\left[\begin{array}{c|c|c|c}1&0&\frac{A}{\omega}(\sin y-\sin x)&\frac{A}{\omega^2}[(y-x)\sin y+(\cos y-\cos x)]\\\hline0&1&-\frac{A}{\omega}(\cos y-\cos x)&-\frac{A}{\omega^2}[(y-x)\cos y-(\sin y-\sin x)]\\\hline\frac{A}{\omega}(\sin y-\sin x)&-\frac{A}{\omega}(\cos y-\cos x)&\frac{2A^2}{\omega^2}[1-\cos(y-x)]&\frac{A^2}{\omega^3}(y-x)[1-\cos(y-x)]\\\hline\frac{A}{\omega^2}[(y-x)\sin y+(\cos y-\cos x)]&-\frac{A}{\omega^2}[(y-x)\cos y-(\sin y-\sin x)]&\frac{A^2}{\omega^3}(y-x)[1-\cos(y-x)]&\frac{A^2}{\omega^4}\{(y-x)-2(y-x)\cdot\sin(y-x)+2[1-\cos(y-x)]\}\end{array}\right] \tag{43}$$

Now from Eqs. (37) and (42)

$$P_4^{-1}(t) = \int_0^t g_4(\tau,t)\,d\tau = \frac{1}{\omega}\int_0^x g_4^*(y,x)\,dy \tag{44}$$

Thus, using Eq. (43) in the integration, the following is obtained:

$$P_4^{-1}(t) = \frac{1}{\sigma_v^2}\begin{bmatrix} \frac{x}{\omega} & 0 & -\frac{A}{\omega^2}(x\cdot sx+cx-1) & -\frac{A}{\omega^3}(x\cdot cx+x-2sx) \\ 0 & \frac{x}{\omega} & -\frac{A}{\omega^2}(sx-x\cdot cx) & -\frac{A}{\omega^3}(x\cdot sx+2cx-2) \\ -\frac{A}{\omega^2}(x\cdot sx+cx-1) & -\frac{A}{\omega^2}(sx-x\cdot cx) & \frac{2A^2}{\omega^3}(x-sx) & \frac{A^2}{\omega^4}(-\frac{x^2}{2}+x\cdot sx-1+cx) \\ -\frac{A}{\omega^3}(x\cdot cx+x-2sx) & -\frac{A}{\omega^3}(x\cdot sx+2cx-2) & \frac{A^2}{\omega^4}(-\frac{x^2}{2}+x\cdot sx-1+cx) & \frac{A^2}{\omega^5}(\frac{x^3}{3}+2x\cdot cx+2x-4sx) \end{bmatrix} \tag{45}$$

Division of the 3,3 and 4,4 cofactors of $P_4^{-1}(t)$ by the determinant of the matrix yields, respectively,

$$\sigma_{\phi_D}^2 = \frac{\omega^3\sigma_v^2}{A^2}\,\frac{\frac{1}{3}x^5+4sx\cdot x^2-8(1-cx)x}{(1/12)x^6+\frac{1}{3}(1-cx)x^4+4sx\cdot x^4-(1-cx)(9-cx)x^2-8sx(1-cx)x+16(1-cx)^2} \tag{46}$$

and

$$\sigma_{\epsilon_D}^2 = \frac{\omega^5\sigma_v^2}{A^2}\,\frac{x^3-2(1-cx)x}{(1/12)x^6+\frac{1}{3}(1-cx)x^4+4sx\cdot x^4-(1-cx)(9-cx)x^2-8sx(1-cx)x+16(1-cx)^2} \tag{47}$$

For comparison we turn now to the axial acceleration maneuver.

Axial Maneuver

When the components of the axial acceleration which are given in Eqs. (15) are substituted into Eq. (40) the following is obtained:

$$F_4(t) = \begin{bmatrix} 0 & 0 & 0 & 0 \\ 0 & 0 & -A & 0 \\ 0 & 0 & 0 & 1 \\ 0 & 0 & 0 & 0 \end{bmatrix} \tag{48}$$

It can be easily shown that the corresponding transition matrix is as follows:

$$\Psi_4(t,t_0) = \begin{bmatrix} 1 & 0 & 0 & 0 \\ 0 & 1 & A(t_0-t) & \frac{1}{2}A(t_0-t)^2 \\ 0 & 0 & 1 & (t_0-t) \\ 0 & 0 & 0 & 1 \end{bmatrix} \tag{49}$$

and hence the integrand of Eq. (37) is

$$g_4(\tau,t) = \frac{1}{\sigma_v^2}\begin{bmatrix} 1 & 0 & 0 & 0 \\ 0 & 1 & -A(\tau-t) & -\frac{1}{2}A(\tau-t)^2 \\ 0 & -A(\tau-t) & A^2(\tau-t)^2 & \frac{1}{2}A^2(\tau-t)^3 \\ 0 & -\frac{1}{2}A(\tau-t)^2 & \frac{1}{2}A^2(\tau-t)^3 & \frac{1}{4}A^2(\tau-t)^4 \end{bmatrix} \tag{50}$$

Following Eq. (37), the integration of Eq. (50) yields

$$P_4^{-1}(t) = \frac{1}{\sigma_v^2}\begin{bmatrix} t & 0 & 0 & 0 \\ 0 & t & \frac{1}{2}At^2 & -(1/6)At^3 \\ 0 & \frac{1}{2}At^2 & \frac{1}{3}A^2t^3 & -\frac{1}{8}A^2t^4 \\ 0 & -(1/6)At^3 & -\frac{1}{8}A^2t^4 & (1/20)A^2t^5 \end{bmatrix} \tag{51}$$

and the division of the 3,3 and 4,4 cofactors of $P_4^{-1}(t)$ by the determinant of the matrix yields, respectively

$$\sigma_{\phi_D}^2 = 192\frac{\omega^3\sigma_v^2}{A^2}\,\frac{1}{x^3} \tag{52}$$

and

$$\sigma_{\phi_D}^2 = 720\frac{\omega^5\sigma_v^2}{A^2}\,\frac{1}{x^5} \tag{53}$$

where, as in Eq. (42), $x=\omega t$.

Note that for large x, i.e., for large t, Eq. (52) decays as $1/t^3$ while Eq. (46), as $1/t$. Also, Eq. (53) decays as $1/t^5$ while Eq. (47), as $1/t^3$. In other words, as in the third-order model, the trend in the reduction of $\sigma_{\phi_D}^2$ for large t is like $1/t^3$ for the axial acceleration maneuver while it is only $1/t$ for the lateral acceleration maneuver. In addition, the reduction in $\sigma_{\epsilon_D}^2$ is like $1/t^5$ for the axial acceleration maneuver while it is only like $1/t^3$ for the lateral acceleration maneuver. This again establishes the observation that whenever the third or fourth order models are adequate (i.e., in cases a, b, and c of group

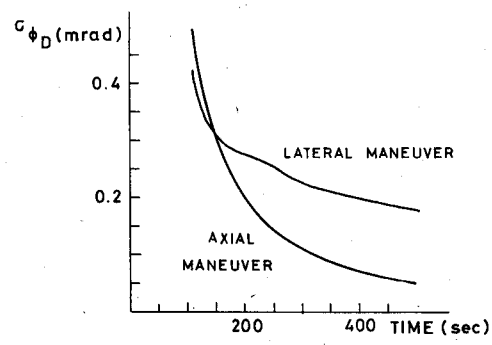

Fig. 3 The standard deviation of the azimuth misalignment estimation error derived from the fourth-order analytic model.

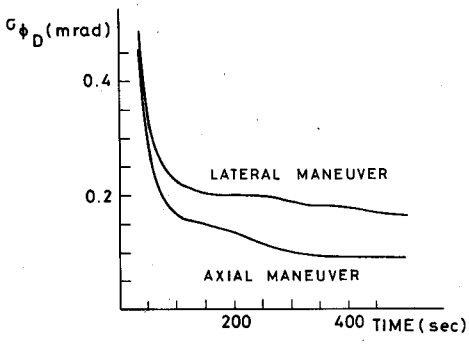

Fig. 4 The standard deviation of the azimuth misalignment estimation error derived from the simulation of case b.

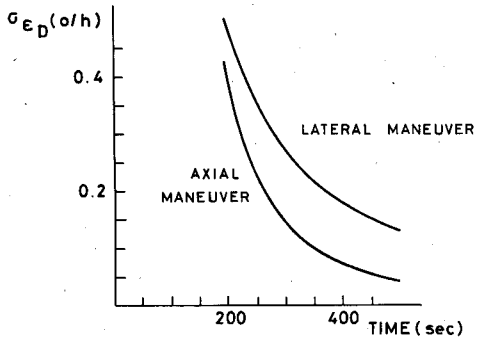

Fig. 5 The standard deviation of the azimuth gyro constant drift rate estimation error derived from the fourth-order analytic model.

number two) the axial acceleration maneuver is superior to the lateral acceleration maneuver in IFA even without the final cruising segment.

To illustrate the difference between the lateral and axial maneuvers in the estimation of ϕ_D, as indicated by this analytic model, we plot, in Fig. 3, σ_{ϕ_D} which is given by Eqs. (46) and (52). To see the correspondence between these analytic results and simulation results, we plot, in Fig. 4, σ_{ϕ_D} of the lateral maneuver and that of the axial maneuver, both obtained from the covariance simulation program. The particular initial conditions which were used in the simulation runs were chosen to make these example runs belong to case b in group number two for which the suitable analytic model is indeed the fourth-order one. Similarly in Figs. 5 and 6 we illustrate the results obtained for the estimation of the azimuth gyro constant drift from the analytic model and the covariance simulation runs respectively. Accordingly, Fig. 5 represents the difference between the lateral and axial maneuvers in the estimation of ϵ_D, as indicated by the analytic model [Eqs. (45) and (53)]. For comparison we plot in Fig. 6 the same quantities as obtained from the simulation that

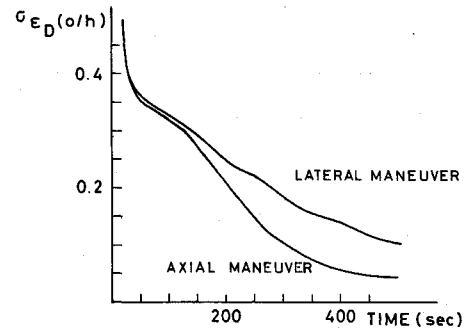

Fig. 6 The standard deviation of the azimuth gyro constant drift rate estimation error derived from the simulation of case b.

generated the plots of Fig. 4. All the numerical values for this simulation are the same as those which were used to generate the plots of Fig. 2 besides the following initial conditions:

$$\sigma_{\epsilon_N} = \sigma_{\epsilon_E} = 2 \text{ deg/h} \qquad \sigma_{\phi_N} = \sigma_{\phi_E} = 1 \text{ min} \qquad \sigma_{\phi_D} = 3 \text{ min}$$

Additional simulation runs were made which belong to case c of group number two. The outcomes of these runs also fit the analytic results obtained from the fourth-order model.

Discussion

If the INS major errors during the IFA process are the azimuth misalignment angle and the aximuth gyro constant drift rate, we say that the IFA problem is a fourth-order planar problem. In such a case, the fourth-order model describes quite accurately the decay of the azimuth misalignment angle and that of the azimuth gyro constant drift rate during the planar maneuvers. If the azimuth gyro constant drift rate happens to be small, then the IFA problem is a third-order planar problem and is well described by the third-order model. It was shown that if the IFA problem is a planar one, axial acceleration is superior to a lateral one already at the end of the accelerating segment of the IFA trajectory. This conclusion holds regardless of the order of the planar problem.

If at the beginning of the IFA all the gyro drift rates are relatively small, then during the cruising phase of the IFA the tilt errors are estimated and at the outset of the accelerating segment of the IFA trajectory the IFA is a third-order planar problem. We designated this case as case a of group number two. If at the beginning of the IFA the two horizontal gyro drift rates are still relatively small but the azimuth gyro constant drift rate is large, we still encounter a planar problem at the beginning of the maneuver; however, now it is a fourth-order one. This case was designated as case c of group number two.

If at the start of the IFA the gyro constant drift rates are not small enough, there is still a chance that the two horizontal drifts will be estimated during the cruising phase of the IFA such that at the beginning of the maneuver these drifts will be smaller than the azimuth gyro constant drift rate. For this to happen, though, the following two conditions have to exist at the outset:

$$\dot{L}\phi_D \ll \epsilon_D \qquad \tilde{\Omega}_N \phi_D \ll \epsilon_D \tag{54}$$

where, as before, $\tilde{\Omega}_N$ denotes the north component of the local level north-pointing coordinate system angular turning rate with respect to an inertial space. This is explained as follows. Immediately at the outset of the cruising part of the IFA trajectory the initial tilt errors are eliminated. Then, from Eq. (1),

$$\dot{\phi}_N \simeq \dot{L}\phi_D + \epsilon_N \qquad \dot{\phi}_E \simeq \tilde{\Omega}_N \phi_D + \epsilon_N \tag{55}$$

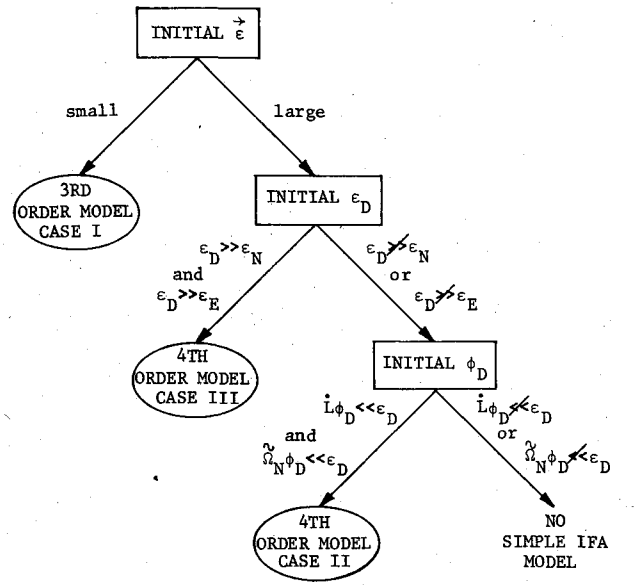

Fig. 7 Flow chart presentation of the division into the various azimuth alignment cases.

Since $\dot{L}\phi_D$ and $\tilde{\Omega}_N\phi_D$ are practically constant, they have a signature similar to that of ϵ_N and ϵ_E, respectively. Consequently they impair the observability of ϵ_N and ϵ_E when the filter attempts to estimate them through the measurement of v_N and v_E. If, however,

$$\dot{L}\phi_D \ll \epsilon_N \quad \text{and} \quad \tilde{\Omega}_N\phi_D \ll \ll \epsilon_E \tag{56}$$

then ϵ_N and ϵ_D are estimated down to the level of $\dot{L}\phi_D$ and $\tilde{\Omega}_N\phi_D$, respectively. Now if this level is much lower than ϵ_D; that is, if the conditions spelled out in Eq. (54) are met, then at the start of the accelerating part of the trajectory, the IFA is again a fourth-order planar problem. This case was designated as case b of group number two. Note that the conditions in Eq. (54) are the conditions of Eq. (8). If none of the preceding conditions exist; that is, if no certain special relations exist among the misalignments and the drifts, there exists no simple IFA model. The flow chart in Fig. 7 illustrates the division into the various cases.

Conclusions

A full-order covariance simulation of the two kinds of maneuvers revealed the following facts:

1) Azimuth misalignment is usually smaller at the end of the baseline IFA trajectory when the axial maneuver is used.

2) When azimuth misalignment is observed during, and particularly, at the end of the maneuver, axial maneuver is superior only when certain initial conditions are met.

3) The conditions necessary for the axial maneuver to be superior in item 2 (above) are the conditions that yield a planar problem at the beginning of the maneuver. We divided these conditions into three cases of initial conditions. All the IFA problems which fall within one of these cases are said to belong to group number two.

We could not find an analytic proof of the claim that axial maneuver is always superior. There is a heuristic argument to support it but this argument does not yield quantitative results, nor does it reveal the superiority, in certain cases, of the lateral acceleration maneuver when azimuth misalignment is observed during, and at the end of the maneuver, and, although not discussed in this work, it cannot be used to compare an alternating axial acceleration maneuver with any other lateral maneuver.

We succeeded, however, in finding two analytic models to describe the behavior of the IFA problems which belong to group number two. The third-order model describes the behavior of the azimuth misalignment when the azimuth gyro drift rate is negligible. When the latter is not negligible, the fourth-order model is the suitable one.

Bar G385

References

[1] Doty, R.L. and Nease, R.F., "Initial Condition and Alignment," *Inertial Guidance,* edited by G.R. Pitman, Wiley, New York, 1962.

[2] Broxmeyer, C., *Inertial Navigation Systems,* McGraw-Hill, New York, 1964.

[3] Sutherland, A.A., Jr., "The Kalman Filter in Transfer Alignment of Inertial Guidance Systems," *Journal of Spacecraft and Rockets,* Vol. 5, Oct. 1968, pp. 1175-1180.

[4] Baziw, I. and Leondes, C.T., "In-Flight Alignment and Calibration of IMU," Parts I and II, *IEEE Transactions,* Vol. AES-5, July 1972, pp. 539-465.

[5] Lorell, K.R., "Use of Calibration Maneuvers for Improved Performance of Strapdown Attitude Reference Systems," *Journal of Spacecraft and Rockets,* Vol. 13, Jan. 1976, pp. 31-36.

[6] Fagan, J.H., Kasper, J.F., Jr., Bongiovanni, P.L., and Sutherland, A.A., Jr., "Strapdown IMU Alignment and Initialization on a Moving Base," The Analytic Sciences Corporation, Reading, Mass., Rept. TR-182-3, Sept. 1969.

[7] Schultz, R.L. and Keyes, C.L., "Airborn IRP Alignment Using Acceleration and Angular Rate Matching," *Proceedings of JACC,* 1973, pp. 427-436.

[8] Kraemer, J.W., Roessler, N.J. and Brandin, D.M., "In-Flight Alignment/Calibration Techniques for Unaided Tactical Guidance," *Proceedings of the National Aerospace and Electronics Conference,* Dayton, Ohio, pp. 705-711.

[9] Benson, D.O., "A Comparison of Two Approaches to Pure-Inertial and Doppler Inertial Error Analysis," *IEEE Transactions,* Vol. AES-11, July 1975, pp. 447-454.

[10] Gelb, A., *Applied Optimal Estimation,* M.I.T. Press, Cambridge, Mass., 1974, p. 131.

[11] Bryson, A.E., Jr. and Ho, Y.C., *Applied Optimal Control,* Blaisdell, Waltham, Mass., 1969, p. 370.